The Cryosphere
Discussions

Open Access

Orientation dependent glacial changes at the Tibetan Plateau derived from 2003–2009 ICESat laser altimetry

V. H. Phan[1,2], R. C. Lindenbergh[1], and M. Menenti[1]

[1]Department of Geosciences and Remote Sensing, Delft University of Technology, Delft, the Netherlands
[2]Department of Geomatics Engineering, Ho Chi Minh City University of Technology, HCM city, Vietnam

Correspondence to: V. H. Phan (phanhienvu@gmail.com)

Discussion Paper | Discussion Paper | Discussion Paper | Discussion Paper |

TCD

8, 2425–2463, 2014

Glacial vertical changes at the Tibetan Plateau

V. H. Phan et al.

Title Page

Abstract | Introduction

Conclusions | References

Tables | Figures

|◄ | ►|

◄ | ►

Back | Close

Full Screen / Esc

Printer-friendly Version

Interactive Discussion

Title Page

Abstract	Introduction
Conclusions	References
Tables	Figures

|◄ ►|

◄ ►

Back Close

Full Screen / Esc

Printer-friendly Version

Interactive Discussion

Abstract

Monitoring glacier changes is essential for estimating the water mass balance of the Tibetan Plateau. Recent research indicated that glaciers at individual regions on the Tibetan Plateau and surroundings are shrinking and thinning during the last decades. Studies considering large regions often ignored however impact of locally varying weather conditions and terrain characteristics on glacial evolution, due to orographic precipitation and variation in solar radiation. Our hypothesis is therefore that adjacent glaciers of opposite orientation change in a different way. In this study, we exploit ICE-Sat laser altimetry data in combination with the SRTM DEM and the GLIMS glacier mask to estimate glacial vertical change trends between 2003 and 2009 on the whole Tibetan Plateau. Considering acquisition conditions of ICESat measurements and terrain surface characteristics, annual glacial elevation trends were estimated for 15 different settings. In the final setting, we only include ICESat elevations acquired over terrain that has a slope of below 20° and a roughness at the footprint scale of below 15 m. Within this setting, 90 glacial areas could be distinguished. The results show that most of observed glacial areas on the Tibetan Plateau are thinning, except for notably glaciers in the Northwest. In general, glacial elevations on the whole Tibetan Plateau decreased at an average rate of -0.17 ± 0.47 m per year ($\mathrm{m\,a^{-1}}$) between 2003 and 2009, but note that the size, distribution, and representativeness of the observed glacial areas are not taken into account. Moreover, the results show that glacial elevation changes indeed strongly depend on the relative position in a mountain range.

1 Introduction

The Tibetan Plateau has steep and rough terrain and contains $\sim 37\,000$ glaciers, occupying an area of $\sim 56\,560\,\mathrm{km^2}$ (Li, 2003). Recent studies report that the glaciers have been retreating significantly in the last decades. According to Yao et al. (2012), the amount of glacier change in the last 30 years is location dependent, with the

largest reduction in glacial length and area occurring in the Himalayas (excluding the Karakoram). Sorg et al. (2012) showed that glacier shrinkage has also occurred at the Tien Shan Mountains in the Northwest of the Tibetan Plateau during the period between 1950 and 2000. As reported in Wang et al. (2011), 910 glaciers in the Middle Qilian Mountain Region have rapidly reduced in area between 1956 and 2003, with a mean reduction of $0.10\,\text{km}^2$ per individual glacier, corresponding to an average rate of $2127\,\text{m}^2\,\text{a}^{-1}$. In addition to generating a glacier inventory for the western Nyaiqentanglha Range for the year ~ 2001 based on Landsat ETM+ and SRTM3 DEM data, Bolch et al. (2010) reported that the glacier area in that region decreased by $-6.1\,\% \pm 3\,\%$ between 1976 and 2001 and glaciers continued to shrink during the period 2001–2009. Recently, Tian et al. (2014) semi-automatically delineated the glacier outlines of ~ 1990, ~ 2000 and ~ 2010 in the Qilian Mountains using Landsat imagery with the help of ASTER GDEM and SRTM DEM elevations, and after combining their results with previous studies found that the total glacier area shrank by $30\,\% \pm 8\,\%$ between 1956 and 2010. Similarly using Landsat images between 2004 and 2011 and topographic maps in 1970s, Wei et al. (2014) reported that the total glacier area at the inner Tibetan Plateau decreased at a rate of $0.27\,\%\,\text{a}^{-1}$. In addition, glaciers in the Tuotuo River basin, the source of the Yangtze River in the inner plateau, have also retreated between 1968 and 2002 (Zhang et al., 2008) as have glaciers in the Mt. Qomolangma (Mt. Everest) region in the Himalayas in the last 35 years (Ye et al., 2009). Most of the above results were analyzed from topographic maps, in situ measurements, and optical remotely sensed images during the observed periods. Recently, however, new remote sensing techniques such as interferometry and radar/laser satellite altimetry have been used for research on glacier and ice-sheet changes.

Between 2003 and 2009 the Geoscience Laser Altimeter System (GLAS) on board of the Ice Cloud and land Elevation Satellite (ICESat) obtained world-wide elevation profiles during 18 one-month campaigns. Measurements were acquired every $\sim 170\,\text{m}$ along track with a footprint diameter of $70\,\text{m}$ (Schutz, 2002). The ICESat mission provided multi-year elevation data that were mostly used to study ice sheet mass balance

over polar areas. However, recently the ICESat data have also been exploited to monitor glaciers in mountain regions such as Himalayas, Alps and the Tibetan Plateau. Kaab et al. (2012) quantified the glacial thinning in the Hindu Kush-Karakoram-Himalaya region from 2003 to 2008, based on the ICESat/GLAS data and the Shuttle Radar Topography Mission (SRTM) Digital Elevation Model. Similarly using ICESat/GLAS data and digital elevation models including SRTM DEM, Advances Spaceborne Thermal Emission and Reflection Radiometer Global Digital Elevation Model (ASTER GDEM) and airphoto DEMs, Kropacek et al. (2013) estimated volume changes of the Aletsch Glacier in the Swiss Alps by two approaches based on elevation differences with respect to a reference DEM and elevation differences between close by tracks. Estimating elevation change rates for high-mountain Asian glaciers based on ICESat/GLAS data is part of regional glacier mass budget studies all over the world (Gardner et al., 2013). In addition, Neckel et al. (2014) applied a method similar to Kaab et al. (2012) for estimating glacier mass changes at eight glacial sub-regions on the Tibetan Plateau between 2003 and 2009. The results indicated that most of the glacial sub-regions had a negative trend in glacial elevation change, excluding one sub-region at the western Mt. Kunlun in the north-west of the Tibetan Plateau.

The glacial elevation changes on the Tibetan Plateau and surroundings obtained from the ICESat/GLAS data provided useful information about the status of glacial sub-regions between 2003 and 2009. However, sampled glacial sub-regions were relative large. As a consequence, the glacial conditions were not homogeneous, due to e.g. orographic precipitation and variation in solar radiation. The significant influence of climatic parameters (Bolch et al., 2010) and spatial variability (Quincey et al., 2009) on glacial change rates has already been demonstrated for several individual glaciers on the Tibetan Plateau. In addition, the quality of ICESat elevations is known to be strongly dependent on terrain characteristics. Therefore, in this paper, we exploit ICESat/GLAS data for monitoring glacial elevation changes on the whole Tibetan Plateau, identifying sampled glacial areas based on ICESat footprints and glacier orientation. In addition, we explore the ICESat/GLAS data by setting and applying criteria impacting the quality

Glacial vertical changes at the Tibetan Plateau

V. H. Phan et al.

Title Page

Abstract	Introduction
Conclusions	References
Tables	Figures

Back | Close

Full Screen / Esc

Printer-friendly Version

Interactive Discussion

of footprints including acquisition condition and terrain surface characteristics. The results are expected to complement to previously estimated water level changes of the Tibetan lakes (Zhang et al., 2011; Phan et al., 2012). Using additional explicit runoff relations between glaciers and lakes (Phan et al., 2013), correlations between glacial and lake level changes can be determined to improve understanding of water balance on the Tibetan Plateau.

2 Data and methods

In this section, we describe input elevation data and glacier outlines. Then we define and build a dataset for monitoring glacial elevation changes. Finally we clean the dataset and estimate temporal elevation trends of sampled glaciers on the Tibetan Plateau.

2.1 Data

Main data sources used to estimate glacial elevation changes at the Tibetan Plateau consist of ICESat laser altimetry data, the Global Land Ice Measurements from Space (GLIMS) glacier mask and the SRTM digital elevation model. The ICESat/GLA14 data supports land surface elevations between 2003 and 2009. The GLIMS glacier outlines represent the glacial regions on the Tibetan Plateau. The SRTM data shows land surface elevations in 2000, used as a base map to be compared with later elevations derived from the ICESat/GLA14 data. To integrate them, all these data are projected onto the World Geodetic System 1984 (WGS84) in horizontal and the Earth Gravitational Model 2008 (EGM2008) in vertical.

2.1.1 ICESat/GLA14 data

The ICESat/GLAS products are provided by the National Snow and Ice Data Center (NSIDC). Here we exploit the level-2 GLA14 data (Zwally et al., 2011), supporting

global land surface altimetry between 2003 and 2009. The GLA14 data is distributed in binary format and is converted into ASCII columns by the NSIDC GLAS Altimetry elevation extractor Tool (NGAT). The geospatial accuracy of each footprint is reported as ∼ 5 m in horizontal and ∼ 10 cm in vertical for slopes below 1° (Schutz, 2002). The vertical accuracy is strongly dependent on terrain characteristics. In this study, necessary measurements of each footprint extracted from the GLA14 data consist of acquisition time, latitude, longitude, elevation above WGS84, EGM2008 geoid height, saturation correction flag, and number of peaks. The saturation correction flag indicates if elevation data was possibly affected by saturation effects. The number of peaks in the Gaussian waveform decomposition directly relates to land surface geometry (Duong et al., 2006). For each ICESat campaign, the ASCII data are converted into the GIS shapefile format, using the location of each footprint. Figure 1 shows the ICESat L2D-campaign tracks from 25 November to 17 December 2008 crossing over the Tibetan Plateau.

2.1.2 SRTM DEM

The Shuttle Radar Topography Mission was flown in February 2000 and collected the first ever high resolution near-global digital elevation data. In this study, we use the SRTM 90 m DEM, produced by NASA (Jarvis et al., 2008). This DEM has a resolution of 90 m at the equator corresponding to 3-arc seconds and is distributed in 5° × 5° tiles. To cover the full Tibetan Plateau, 20 SRTM DEM tiles are concatenated, as shown in Fig. 1. The tiles are available in both ArcInfo ASCII and GeoTiff format. The digital elevation data were stored in a grid as $m \times n$ matrix. The data is projected in a Geographic (latitude/longitude) projection, with the WGS84 horizontal datum and the EGM96 vertical datum. The vertical error of the DEM's is reported to be less than 5 m on relative flat areas and 16 m on steep and rough areas (Zandbergen, 2008).

Glacial vertical changes at the Tibetan Plateau

V. H. Phan et al.

Title Page

Abstract | Introduction

Conclusions | References

Tables | Figures

|◄ | ►|

◄ | ►

Back | Close

Full Screen / Esc

Printer-friendly Version

Interactive Discussion

2.1.3 GLIMS glacier outlines

The GLIMS project is a project designed to monitor the world's glaciers, primarily using data from optical satellite instruments. Now over 60 institutions world-wide are involved in GLIMS for inventorying the majority of the world's estimated 160 000 glaciers. These glaciers are distributed in GIS shapefile format and are referenced to the WGS84 datum. In this study, we downloaded the glacier mask presenting glacial outlines on the Tibetan Plateau, submitted by Li (2003) – Chinese Academy of Sciences, as shown in Fig. 1. The glacier mask is based on aerial photography, topographic maps and in situ measurements. The product was released on 21 July 2005, but the state of the glaciers is expected to represent the situation in 2002 (Shi et al., 2009). Each glacier is represented by a polygonal vector with attributes such as identication code, area, width, length, min elevation, max elevation, and name.

2.2 Methods

To estimate a temporal trend in glacial elevation, we compare elevations obtained from the ICESat/GLA14 data to the SRTM DEM over glacial areas. Differences between 2003–2009 GLAS elevations and 2000 SRTM elevations may correspond to glacial changes. However, the vertical accuracy of each ICESat footprint strongly depends on terrain surface characteristics, so we have to remove uncertain footprints before the estimation. In this section, firstly we estimate surface slope and roughness from the SRTM DEM data. Secondly we determine those glacial areas that are sufficiently sampled. Thirdly we identify valid elevation changes for each glacial area. Finally we estimate glacial elevation trends per area.

2.2.1 Estimating surface slope and roughness from SRTM DEM

Based on the SRTM DEM, the terrain surface parameters slope S and roughness R are estimated, using a 3 × 3 kernel scanning over all pixels of the grid, as illustrated in

Fig. 2. For each pixel, the slope S in decimal degrees is locally estimated by Eq. (1) (Verdin et al., 2007; Shi et al., 2013).

$$S = \frac{180}{\pi} \times \arctan \sqrt{\left(\frac{dz}{dx}\right)^2 + \left(\frac{dz}{dy}\right)^2} \tag{1}$$

$$\frac{dz}{dx} = \frac{(h_3 + 2 \times h_6 + h_9) - (h_1 + 2 \times h_4 + h_7)}{8 \times \Delta lon} \tag{2}$$

$$\frac{dz}{dy} = \frac{(h_7 + 2 \times h_8 + h_9) - (h_1 + 2 \times h_2 + h_3)}{8 \times \Delta lat} \tag{3}$$

Here, Δlat and Δlon are the width and the height of a grid cell in meters, estimated by distance Eq. (4) (Sinnott, 1984).

$$d = r \times 2 \times a \tan 2(\sqrt{a}, \sqrt{1-a})$$

$$a = \sin^2\left(\frac{\varphi_2 - \varphi_1}{2}\right) + \cos(\varphi_1) \times \cos(\varphi_2) \times \sin^2\left(\frac{\lambda_2 - \lambda_1}{2}\right) \tag{4}$$

Here, d is the shortest distance over the earth's surface – the "as-the-crow-flies" distance between the two points (λ_1, φ_1) and (λ_2, φ_2) in radians in a geographic coordinate system and r is the earth's radius (mean radius = 6371 km).

The roughness R in meters is defined as the root mean square of the differences $\hat{e}_i$, $i = 1/9$, between the grid heights and the local 3×3 plane, best fitting in the least squares sense, Lay (2003) and Shi et al. (2013).

$$R = \sqrt{\frac{\sum_{i=1}^{i=9} \hat{e}_i^2}{9}} \tag{5}$$

2.2.2 Determining a sampled glacial area

Because of the orbital configuration of ICESat and its along track only sampling ability, Tibetan glacial areas are only sampled sparsely by ICESat. In addition, elevation

Full Screen / Esc

Printer-friendly Version

Interactive Discussion

changes on these mountain glaciers are expected to be affected significantly by the orientation and face of the corresponding mountain range. For example, the South face of the Himalayas is experiencing more precipitation than the North face, while on the other hand North faces experience less incoming sunlight. Therefore we decided to

5 group nearby glaciers having similar orientation into one sampled glacial area while, on the other hand, glaciers on different sides of a mountain range ridge were grouped into different areas. First we extracted footprints of all ICESat campaigns within the GLIMS glacier outlines, as illustrated in Fig. 3. Then each glacial area outline was manually determined, by considering the locations of the glaciers and the ICESat footprints. For

10 example, in Fig. 3 the ICESat-sampled glaciers having a northern orientation were grouped into one glacial area, A, while those on the other site of the mountain ridge were grouped into another glacial area, B. Finally each glacial area was coded by an identification number.

2.2.3 Identifying glacial elevation differences

15 For each glacial area, elevation changes are represented by differences between ICE-Sat elevations and the reference SRTM DEM. Each elevation difference depends on the characteristics of the terrain illuminated by the ICESat pulse and the characteristics of the ICESat measurement itself. In this study, we assess the quality of each elevation difference, by exploring the set of attributes described in Table 1. For this pur-

20 pose, we extract ICESat footprints within the identified glacial areas and obtain their full attributes.

The elevation difference Δh is defined in Eq. (6), where Δh is in meters above EGM2008.

$$\Delta h = h_{\text{ICESat}} - h_{\text{SRTM}} = (\text{Elev} - \text{GdHt}) - (\text{SRTM\_elev} + 96\_08\_\text{Ht}) \qquad (6)$$

25 An elevation difference is maintained for further analysis if the corresponding ICESat measurement is considered good according to the following criteria. First we select those footprints whose return echo is not or only lightly saturated and moreover have

only one peak in its Gauss decomposition. That is the value of SatFlg should equal 0 or 1, and the value of NumPk should equal 1. A footprint with one mode is expected to correspond to homogeneous land surface. Then we remove footprints affected by clouds. If ICESat footprints are affected by clouds, the elevation variation within one track can be very large, while the altitude difference with other tracks is high (Phan et al., 2012). In this study, if the ICESat elevation difference to the SRTM DEM Δh is larger than 100 m, the footprint is assumed to be affected by clouds and removed from further analysis.

2.2.4 Different settings with respect to slope and roughness

Here we analyze different settings incorporating the terrain surface characteristics slope and roughness. We remove footprints with a slope S bigger than a threshold S_0 and roughness R bigger than a threshold R_0. Applying strict thresholds will result in a relative small number of remaining elevation changes albeit of relatively high quality. A slope S below 10° is always considered good while a slope of over 30° results in an inacceptable bias. The roughness R is estimated directly from the SRTM data, its lower limit of 5 m corresponds to relative flat areas while its upper limit of 15 m corresponds to high relief and rough areas. In the following we consider 15 different settings with slope and roughness values within these outer limits, as described in Table 2. Each record in Table 2, corresponding to one such setting, also summarizes the corresponding results of glacial elevation changes for the whole Tibetan Plateau between 2003 and 2009, as determined by the following steps.

2.2.5 Obtaining glacial elevation changes

For each observed glacial area, elevation differences all are time-stamped by the ICESat-sampling time. The ICESat sampling time t_i is defined per ICESat track, where one track is sampling a glacial area by several consecutive individual footprints. The average elevation difference $\overline{\Delta h_i}$ is considered representative for the height of the glacial

Title Page

Abstract | Introduction

Conclusions | References

Tables | Figures

|◄ | ►|

◄ | ►

Back | Close

Full Screen / Esc

Printer-friendly Version

Interactive Discussion

area above the SRTM base map at ICESat-sampling time t_i. The average elevation difference $\overline{\Delta h_i}$ and its standard deviation s_i is computed using Eqs. (7) and (8), where k is the number of ICESat footprints in the track that are sampling the glacial area at ICESat-sampling time t_i and Δh_{ij} is the jth elevation difference, $j = 1/k$.

$$\overline{\Delta h_i} = \frac{1}{k} \sum_{j=1}^{j=k} \Delta h_{ij} \tag{7}$$

$$s_i = \sqrt{\frac{1}{k} \sum_{j=1}^{j=k} (\Delta h_{ij} - \overline{\Delta h_i})^2} \tag{8}$$

Each ICESat-sampling time t_i is considered as an epoch in the time series used to estimate a temporal trend using linear regression. Here we only use the average elevation difference $\overline{\Delta h_i}$ for the linear trend if its standard deviation s_i is less than a threshold Std_0 and the number of ICESat footprints k is at least six footprints. The threshold Std_0 is defined to be equal to the roughness threshold R_0 for each scenario. To remove unreliable elevation differences, we build an iterative algorithm. That is, if s_i is bigger than Std_0 and $\left| \Delta h_{ij} - \overline{\Delta h_i} \right|$ is maximal for j in $1/k$, the jth elevation difference Δh_{ij} is removed. Then $\overline{\Delta h_i}$ and s_i are re-computed. This process is repeated until s_i drops below Std_0 or k is less than six. In Fig. 4, the values $\overline{\Delta h_i}$ and s_i representing glacial elevation changes and their standard deviations are shown between 2003 and 2009 for two glacial areas A and B in case that S_0, R_0, and Std_0 are 15°, 10 m, and 10 m, respectively.

2.2.6 Estimating temporal glacial elevation trends

For each glacial area on the Tibetan Plateau, a temporal linear trend is estimated if there are at least six average differences or epochs available, corresponding to at

least six ICESat campaign tracks during the observed period 2003–2009. For example, Fig. 4 shows the distribution of the average differences of the glacial areas A and B between 2003 and 2009. The annual glacial elevation trend is estimated by linear adjustment using Eq. (9) (Teunissen, 2003).

$$\hat{x} = (\mathbf{A}^{\mathsf{T}}\mathbf{A})^{-1}\mathbf{A}^{\mathsf{T}}y \tag{9}$$

Where, $y = \begin{bmatrix} \overline{\Delta h_1} & \overline{\Delta h_2} & \cdots & \overline{\Delta h_n} \end{bmatrix}^{\mathsf{T}}$: the vector of the average elevation differences per epoch.

$x = \begin{bmatrix} x_0 & v \end{bmatrix}$: the vector of parameters of the linear trend, offset x_0 and velocity v.

$\mathbf{A} = \begin{bmatrix} 1 & 1 & \cdots & 1 \\ t_1 & t_2 & \cdots & t_n \end{bmatrix}^{\mathsf{T}}$: the design matrix, in which t_i denotes the ith epoch.

Note that n is required to be at least six epochs.

The velocity v of linear glacial elevation change is obtained from solving Eq. (9) and the root mean square error (RMSE), as standard deviation of residuals, is also computed, using Eq. (10) with the least-square residual vector $\hat{e} = y - \mathbf{A}\hat{x}$. This value consists of a combination of possible data errors and mainly the non-validity of the linear regression model.

$$\mathrm{RMSE} = \sqrt{\frac{\sum\limits_{i=1}^{i=n} \hat{e}_i^2}{n}} \tag{10}$$

In addition, the propagated standard deviation σ_{vv} of the estimated velocity v is given in Eq. (11). This value is considered as the confidence interval for the estimated glacial elevation change.

$$\mathbf{Q}_{\hat{x}\hat{x}} = \begin{bmatrix} \sigma_{x_0 x_0}^2 & \sigma_{x_0 v}^2 \\ \sigma_{v x_0}^2 & \sigma_{vv}^2 \end{bmatrix} = (\mathbf{A}^{\mathsf{T}}\mathbf{Q}_{yy}^{-1}\mathbf{A})^{-1}, \text{ with } \mathbf{Q}_{yy} = \begin{bmatrix} s_1^2 & 0 & 0 & 0 \\ 0 & s_2^2 & 0 & 0 \\ & & \cdots & \\ 0 & 0 & 0 & s_n^2 \end{bmatrix} \tag{11}$$

Here, $\mathbf{Q}_{yy}$ denotes the variance matrix, in which s_i is the standard deviation of the ith average difference.

Continuing to the example of Fig. 4, glacial area A has an elevation decrease of $-1.66 \pm 0.42\,\mathrm{m\,a^{-1}}$ and a RMSE of 3.46 m while glacial area B has an elevation increase of $0.50 \pm 0.31\,\mathrm{m\,a^{-1}}$ and a RMSE of 3.37 m between 2003 and 2009.

3 Results

Following the method above, temporal glacial elevation trends on the whole Tibetan Plateau between 2003 and 2009 are estimated for 15 different settings. The results are shown in Table 2. It indicates that, as expected, the number of observed glacial areas and the RMSEs of the glacial elevation trends increase if the thresholds on slope S_0 and roughness R_0 are relaxed. In practice, the average rates of glacial elevation changes on the whole Tibetan Plateau for the five scenarios from S11 to S15 (all with $R_0 = 15\,\mathrm{m}$) are quite similar. In addition, the number of trends having a RMSE of over 5 m significantly increases when ICESat footprints at slopes of over 20° are incorporated as well. A RMSE of over 5 m could correspond to a large fluctuation in glacial elevation or a bad fit of the linear trend model. In this section we present the results of scenario S13, where S_0 and R_0 equal 20° and 15 m, respectively, because in this case the maximum number of 67 areas with RMSE ≤ 5 m is observed. We assume that ICESat footprints selected for estimation of glacial elevation change given these settings are relatively appropriate given the steep and rough terrain of the Tibetan Plateau and given the quality of the SRTM DEM.

3.1 Overall glacial elevation changes: Tibetan Plateau and its basins

In case that the thresholds $S_0 = 20°$ for terrain slope and $R_0 = 15\,\mathrm{m}$ for roughness are applied the result indicates that 90 glacial areas on the whole Tibetan Plateau are sampled by enough ICESat footprints to estimate elevation change. Also, 67 RMSEs

are below 5 m. For each area, a temporal trend in glacial elevation is estimated, as shown in the Supplement. In Fig. 5, a glacial elevation change rate is symbolized by a red or green disk at a representative location in each observed glacial area. Most of the observed glacial areas in the Himalaya, the Hengduan Mountains and the Tang-gula Mountains experienced a serious glacial elevation decrease. However, at most of the observed areas in the western Kunlun Mountains in the north-west of the Ti-betan Plateau, glaciers oriented toward the North were thickening while those oriented toward the South were thinning. In general, glacial elevations on the whole Tibetan Plateau decreased between 2003 and 2009 at an average rate of $-0.17 \pm 0.47 \, \mathrm{m \, a^{-1}}$. This number is obtained by averaging all estimated velocities v and their propagated standard deviations σ_{vv}, but note that the size, distribution and representativeness of the observed glacial areas are not taken into account.

The largest glacial elevation decrease occurred at the Hengduan Mountains, compare Fig. 6. The estimated rate equals $-2.03 \pm 0.73 \, \mathrm{m \, a^{-1}}$ with a RMSE of 0.32 m. The observed glacial area consists of two GLIMS glaciers facing East. Although there are little discrepancies between the GLIMS glacier outlines and the Landsat 8 OLI/TIRS, captured on 13 August 2013, Fig. 6 indicates that glaciers have retreated significantly between ∼ 2002, the time corresponding to the GLIMS database, and 2013. On the other hand, the observed glacial area facing North at Western Mt. Kunlun had an elevation increase rate of $+1.25 \pm 0.51 \, \mathrm{m \, a^{-1}}$ and a RMSE of 3.09 m, as illustrated in Fig. 7. Overlaying the GLIMS glacier mask on the Landsat 8 OLI/TIRS image from 18 September 2013 indicates that in this area the glacier extent is relatively stable.

For each basin belonging to the Tibetan Plateau, an average thinning or thickening rate $\overline{v_B} \pm \overline{\sigma_B}$ is estimated, as average of velocities v and propagated standard deviations σ_{vv}. The result is shown in Table 3. In practice, the rate per basin is of course affected by the area of each glacier within the basin. However, in this study we only estimate trends representative for nearby-glacier groups. A next but far from trivial step would be to design an interpolation scheme taking the sparsely available trends as input and use them to estimate an overall trend while incorporating e.g. the relative location,

orientation, and representativeness of each available trend. Here the area of glaciers is not taken into account when estimating overall glacial rates. The results show that mass loss due to glacier-thinning seems to take place in most of the basins, excluding Tarim Basin. Subsequently, lost or gained water volumes from glaciers by basin are approximately estimated, by multiplying the average glacial vertical change rate with the total glacier area of each basin, as indicated in Table 3.

3.2 Impact of orientation on glacial vertical change

The results indicate that glacial vertical change indeed strongly depends on the relative position in a mountain range. Most glaciers at a North face increase in volume, although some decrease but in that case at a slower rate than its South-facing counterpart. In total, there are 15 pairs of observed glacial areas, i.e. adjacent glacial areas but located at opposite faces of the main mountain ridge, all listed in Table 4. Such situation is illustrated in Fig. 8, showing the western Mt. Kunlun range. The temporal trends between 2003 and 2009 at the North-facing glacial area A equaled $0.69 \pm 0.30\,\mathrm{m\,a^{-1}}$ while at its South-facing counterpart, glacial area B, the trend had opposite sign, equaling $-1.02 \pm 0.29\,\mathrm{m\,a^{-1}}$. Similarly, the glacial elevation change rates at E, facing North, and F, facing Southeast were $0.58 \pm 0.28\,\mathrm{m\,a^{-1}}$ and $-0.29 \pm 0.44\,\mathrm{m\,a^{-1}}$, respectively. On the other hand, the glacial elevation at C, toward the Northeast, was estimated to decrease at a rate of $0.09 \pm 0.30\,\mathrm{m\,a^{-1}}$ while glaciers in area D, toward the Southwest, thinned at a rate of $-0.29 \pm 0.20\,\mathrm{m\,a^{-1}}$. A possible explanation is that South-facing glaciers receive much more solar radiation than North-facing glaciers. Even glacial area C, oriented toward the Northeast, faces the sun more than areas A and E. Similarly, glacial area D, oriented toward the Southwest, is receiving less sunlight than glacial areas B and F.

Glacial vertical changes at the Tibetan Plateau

V. H. Phan et al.

Title Page

Abstract	Introduction
Conclusions	References
Tables	Figures

|◄ | ►|

◄ | ►

Back | Close

Full Screen / Esc

Printer-friendly Version

Interactive Discussion

4 Discussions

In this section, we discuss the sensibility of our results with respect to the removing of ICESat footprints based on terrain surface criteria and the GLIMS glacier mask. First we discuss the impact of the terrain surface criteria for assessing the signal quality of the ICESat measurements. Second, the GLIMS glacier mask is static which has some effect on the estimation of glacial elevation. Finally a comparison of our result to previous research is presented.

4.1 Exploring terrain surface criteria

Several large glaciers sampled by ICESat footprints were considered to assess appropriate terrain surface criteria. The following relations were notably studied while determining the thresholds for terrain slope and roughness: elevation difference Δh vs. slope S, roughness R and elevation h_{SRTM}, respectively; and slope S vs. elevation h_{SRTM}. The results are illustrated here for one case study considering a glacier area at the Mt. Guala Mandhata I. The results indicate that elevation differences Δh increase with terrain slope, as illustrated in Fig. 9a. The existence of such a slope bias is already described in Slobbe et al. (2008). Large valley glaciers often have a surface roughness of below 20 m, see Fig. 9b. Also a larger surface roughness will result in a positive bias in the elevation difference.

The relaxation of the slope threshold results in an increase in the number of accepted ICESat tracks sampling a glacial area. This is illustrated in Fig. 10 for an area in the Hengduan Mountains (Table S1, No. 6 in the Supplement). In Fig. 10a, a number of 10 tracks was accepted, given a slope threshold of 15°. Based on these tracks, a trend was estimated with a RMSE of 4.18 m. In Fig. 10b, the slope threshold was relaxed to 25°, resulting in a total number of 13 tracks. But the quality of the final trend (RMSE = 6.39 m) decreases with the increase of the number of tracks. These two examples show some of the impact of the slope and roughness thresholds.

One of the results of Kaab et al. (2012) and Neckel et al. (2014) were annual glacial vertical trends for defined regions. These trends were directly estimated from all elevation differences between ICESat elevations and the reference SRTM DEM on glacier areas, after removing footprints affected by clouds. This method ensures the availability of sufficient ICESat footprints to estimate trends in glacial thickness for relatively large regions. However, it ignores the impact of the high relief terrain characteristics of the Tibetan Plateau and surrounding mountain ranges. In addition, their definition of the sampled regions somehow smoothes out significant signal, as it lumps together glaciers with different characteristics with respect to orography and orientation. Clearly there is a difficult trade-off between using more elevations of less individual quality against using less elevations of better quality.

4.2 State of the GLIMS glacier mask

According to Shi et al. (2009), observations serving as input for the GLIMS glacier mask were obtained from 1978 to 2002, using aerial photographs, topographic maps and in situ measurements. Because of remoteness and harsh climatic conditions on the Tibetan Plateau, it is difficult to make field investigation, therefore the Chinese glacier inventory that was used to establish the GLIMS glacier mask took place at different periods. The inventory was organized per drainage basin. Inventory for example occurred at Mt. Qilian in 1981, at the Inner Plateau in 1988, etc. Positional uncertainty is expressed as a distance of 20 m, i.e. a given location lies within a circle of 20 m radius from the true location. In addition, recent studies (Tian et al., 2014; Wei et al., 2014; Yao et al., 2012; Wang et al., 2011; Ye et al., 2009; Zhang Y. et al., 2008) report that the total glacier area on the Tibetan Plateau is shrinking. Therefore, in this study some ICESat footprints acquired between 2003 and 2009 will fall within the GLIMS glacier outlines but are not sampling a real glacier anymore. This will affect the average elevation difference $\overline{\Delta h_i}$ at the ICESat-sampling time i. However, the number of such footprints within the same ICESat track is not large because the along track distance

between consecutive footprints is approximately 170 m, and criteria on terrain surface are in place to remove uncertain footprints.

To further improve the glacial vertical change trends derived from ICESat/GLAS data, two techniques could be applied. First the glacier mask could be checked for each ICESat campaign using contemporary spectral (e.g. Landsat 8) or SAR data (e.g. Sentinel 1). Alternatively, classification techniques could be applied to the ICESat full waveform signals (GLA01 or GLA06 product) to verify if a ICESat signal is sampling snow, ice or rock (Molijn et al., 2011). Applying both types of analysis for the complete Tibetan Plateau is quite labor intensive however. Kaab et al. (2012) and Neckel et al. (2014) exploited the most cloud free Landsat scenes, acquired between 2003 and 2011 to delineate glacier outlines. However, it is difficult to match the acquisition time of ICESat campaigns with Landsat data for the full observed period for the whole Tibetan Plateau.

4.3 Glacial vertical changes for sub-regions

Our result considers annual glacial vertical change trends for relatively small areas. It is interesting to compare it with previous research (Neckel et al., 2014). Neckel et al. (2014) grouped glaciers on the Tibetan Plateau into eight sub-regions, as illustrated in Fig. 11. One of their results consists of annual glacial vertical change trends for each of these eight sub-regions. Accordingly we estimated glacial trends for the same eight sub-regions as well. For each sub-region, a glacial vertical trend $\overline{v_R} \pm \overline{\sigma_R}$ is estimated as average of the vertical change velocities v and propagated standard deviations σ_{vv} of the observed glacial areas within the sub-region. The results are presented in Table 3 and compared to Neckel's Δh trends.

The comparison indicates that sub-regions (A, F, G, and H), relatively densely covered by glaciers, have a similar vertical change trend. Considering the other sub-regions, sub-region D has a somehow similar trend while trends at sub-regions B and C have a relative large disparity. The disparity between sub-regions B and C may be caused by (i) the low number of observed glacial areas and (ii) differences in orientation of the observed glacial areas: sub-region B consists of two South-facing glacial

Title Page

Abstract | Introduction

Conclusions | References

Tables | Figures

|◄ | ►|

◄ | ►

Back | Close

Full Screen / Esc

Printer-friendly Version

Interactive Discussion

areas and one North-facing glacial area while sub-region C consists of three South-facing glacial areas and two North-facing glacial areas. At sub-region E, in case we set $S_0 = 20°$ and $R_0 = 15$ m, the number of ICESat footprints is not enough to estimate a temporal trend. We assume that the total number of observed glacial areas per sub-region and their orientation affect these average glacial vertical change rates. That is, when the number of observed glacial areas is large enough and observed glacial areas located on opposite sides of the main mountain ridge are similarly balanced, the average glacial vertical trend per sub-region is going to be more reliable.

Generally our results are comparable to elevation changes estimated for high-mountain Asia glaciers by Gardner et al. (2013). Both results indicate that most of the glaciers in the Tibetan Plateau are thinning, except for western Mt. Kunlun. The strongest glacier-thinning occurs in the Himalaya range: -0.81 ± 0.46 m a^{-1} (this research) vs. -0.53 ± 0.13 m a^{-1} in western Himalaya, -0.44 ± 0.20 m a^{-1} in central Himalaya and -0.89 ± 0.13 m a^{-1} in eastern Himalaya (Gardner et al., 2013), and in the Hengduan mountains: -0.67 ± 0.58 m a^{-1} (this research) vs. -0.40 ± 0.41 m a^{-1} (Gardner et al., 2013). Glacial vertical changes are near balance in the western and central Tibetan Plateau: -0.05 ± 0.45 m a^{-1} (this research) vs. -0.12 to $+0.16$ m a^{-1} (Gardner et al., 2013). Inversely glaciers in the western Mt. Kunlun are thickening: 0.20 ± 0.45 m a^{-1} (this research) vs. 0.17 ± 0.15 m a^{-1} (Gardner et al., 2013).

4.4 Representativeness of an observed glacial area

A difficult question is to what extent the sparse estimates obtained by ICESat are representative for the full population of the Tibetan Plateau glaciers. This question cannot be answered here but we can assess what part of the glaciers is sampled. For this purpose we determine the ratio κ between glacial area sampled by ICESat footprints and the total glacial area, following Eq. (12).

$$\kappa = \frac{N \times A_F}{A_G} \tag{12}$$

Here N is the total number of accepted ICESat footprints, A_F is the area covered by one ICESat footprint and A_G is the total sampled glacial area.

A glacial area can be considered to be well sampled if the total number of accepted ICESat footprints for an observed glacial area is large and its total area is relatively small. An ICESat footprint with its diameter of 70 m occupies an area A_F of ~ 3850 m^2. For example in Fig. 3, glacial area A occupies 30.6 km^2 and is sampled by 108 accepted ICESat footprints. Therefore A's sample ratio equals 0.0136. Similarly, glacial area B occupies 8.5 km^2 and is sampled by 94 accepted ICESat footprints, so B's sample ratio is 0.0426. In this way the sample ratio for each of 90 observed glacial areas is determined, see Supplement.

Similarly, the sample ratio for all observed glacial areas on the whole Tibetan Plateau could be computed as well. As a result, the total area of 90 observed glacial areas for the whole Tibetan Plateau is 5831.5 km^2 and these glacial areas were sampled by a total number of 16 002 accepted ICESat footprints. Thus in this case the sample ratio equals 0.0106. Note that one location might be sampled by several ICESat footprints from different epochs. That is not taken into account in this first assessment.

5 Conclusions

Exploiting ICESat laser altimetry data, vertical trends of 90 glacial areas on the whole Tibetan Plateau were estimated between 2003 and 2009. By exploring terrain surface criteria slope and roughness, annual glacial vertical trends for the whole Tibetan Plateau were evaluated for 15 different scenarios. The results show that the settings of terrain slope and roughness equaling 20° and 15 m to remove uncertain ICESat footprints, respectively, are appropriate for the steep and rough Tibetan Plateau. In addition, the orientation of glaciers has been taken into account. The study indicated that most of the observed glacial areas in the Himalaya, the Hengduan Mountains and the Tanggula Mountains experienced a serious thinning while in most of the observed areas of the western Kunlun Mountains North-facing glaciers were thickening

Title Page

Abstract | Introduction

Conclusions | References

Tables | Figures

Back | Close

Full Screen / Esc

Printer-friendly Version

Interactive Discussion

while South-facing glaciers were thinning. In addition, glacial elevation changes indeed strongly depend on the relative position in a mountain range. Most North-facing glaciers increase in thickness, although some decrease but in that case at a slower rate than its South-facing counterpart.

Supplementary material related to this article is available online at http://www.the-cryosphere-discuss.net/8/2425/2014/tcd-8-2425-2014-supplement. pdf.

References

Bolch, T., Yao, T., Kang, S., Buchroithner, M. F., Scherer, D., Maussion, F., Huintjes, E., and Schneider, C.: A glacier inventory for the western Nyainqentanglha Range and the Nam Co Basin, Tibet, and glacier changes 1976–2009, The Cryosphere, 4, 419–433, doi:10.5194/tc-4-419-2010, 2010.

Duong, H., Pfeifer, N., and Lindenbergh, R.C: Full waveform analysis: ICESat laser data for land cover classification, in: Proceedings: ISPRS Mid-term Symposium, Remote Sensing: From Pixel to Process, Enschdede, 8–11 May, the Netherlands, 31–35, 2006.

Gardner, A. S., Moholdt, G., Cogley, J. G., Wouters, B., Arendt, A. A., Wahr, J., Berthier, E., Hock, R., Pfeffer, W. T., Kaser, G., Ligtenberg, S. R. M., Bolch, T., Sharp, M. J., Hagen, J. O., van den Broeke, M. R., and Paul, F.: A reconciled estimate of glacier contributions to sea level rise: 2003 to 2009, Science, 340, 852–857, doi:10.1126/science.1234532, 2013.

Jarvis, A., Reuter, H. I., Nelson, A., and Guevara, E.: Hole-filled SRTM for the globe Version 4, available from the CGIAR-CSI SRTM 90 m Database, available at: http://srtm.csi.cgiar.org (last access: 4 April 2014), 2008.

Lay, D. C.: Linear Algebra and its Applications, 3rd Edn., Addison Wesley, USA, 2002.

Li, X.: GLIMS Glacier Database, Boulder, Colorado USA: National Snow and Ice Data Center, doi:10.7265/N5V98602, 2003.

Glacial vertical changes at the Tibetan Plateau

V. H. Phan et al.

Title Page

Abstract	Introduction
Conclusions	References
Tables	Figures

|◄ | ►|

◄ | ►

Back | Close

Full Screen / Esc

Printer-friendly Version

Interactive Discussion

Kaab, A., Berthier, E., Nuth, C., Gardelle, J., and Arnaud, Y.: Contrasting patterns of early twenty-first-century glacier mass change in the Himalayas, Nature, 488, 495–498, 2012.

Kropáček, J., Neckel, N., and Bauder, A.: Estimation of volume changes of mountain glaciers from ICESat data: an example from the Aletsch Glacier, Swiss Alps, The Cryosphere Discuss., 7, 3261–3291, doi:10.5194/tcd-7-3261-2013, 2013.

Neckel, N., Kropacek, J., Bolch, T., and Hochschild, V.: Glacier mass changes on the Tibetan Plateau 2003–2009 derived from ICESat laser altimetry measurements, Environ. Res. Lett., 9, 014009, doi:10.1088/1748-9326/9/1/014009, 2014.

Pavlis, N. K., Holmes, S. A., Kenyon, S. C., and Factor, J. K.: An Earth Gravitational Model to Degree 2160: EGM2008, presented at the 2008 General Assembly of the European Geosciences Union, Vienna, Austria, 13–18 April 2008.

Phan, V.H, Lindenbergh, R. C., and Menenti, M.: ICESat derived elevation changes of Tibetan lakes between 2003 and 2009, Int. J. Appl. Earth Obs., 17, 12–22, 2012.

Phan, V. H., Lindenbergh, R. C., and Menenti, M.: Geometric dependency of Tibetan lakes on glacial runoff, Hydrol. Earth Syst. Sci., 17, 4061–4077, doi:10.5194/hess-17-4061-2013, 2013.

Quincey, D. J., Luckman, A., and Benn, D.: Quantification of Everest region glacier velocities between 1992 and 2002, using satellite radar interferometry and feature tracking, J. Glaciol., 55, 596–606, 2009.

Schutz, B. E.: Laser Footprint Location (Geolocation) and Surface Profiles, Technical Report of Geoscience Laser Altimeter System (GLAS), Center for Space Research, The University of Texas, Austin, 2002.

Shi, J., Menenti, M., and Lindenbergh, R. C.: Parameterization of surface roughness based on ICESat/GLAS full waveforms: a case study on the Tibetan Plateau, J. Hydrometeorol., 14, 1278–1292, doi:10.1175/JHM-D-12-0130.1, 2013.

Shi, Y., Liu, C., and Kang, E.: The glacier inventory of China, Ann. Glaciol., 50, 1–4, 2009.

Sinnott, R. W.: Virtues of the Haversine, Sky Telescope, 68, p. 159, 1984.

Slobbe, D. C., Lindenbergh, R. C., and Ditmar, P.: Estimation of volume change rates of Greenland's ice sheet from ICESat data using overlapping footprints, Remote Sens. Environ., 112, 4204–4213, 2008.

Sorg, A., Bolch, T., Stoffel, M., Solomina. O., and Beniston, M.: Climate change impacts on glaciers and runoff in Tien Shan (Central Asia), Nature Climate Change, 2, 725–731, 2012.

Glacial vertical changes at the Tibetan Plateau

V. H. Phan et al.

Title Page

Abstract	Introduction
Conclusions	References
Tables	Figures

◀◀ ▶▶

◀ ▶

Back Close

Full Screen / Esc

Printer-friendly Version

Interactive Discussion

Teunissen, P. J. G.: Adjustment Theory: an Introduction, VSSD, chapter 2, the Netherlands, 2003.

Tian, H., Yang, T., and Liu, Q.: Climate change and glacier area shrinkage in the Qilian mountains, China, from 1956 to 2010, Ann. Glaciol., 55, 187–197, 2014.

Verdin, K. L., Godt, J. W., Funk, C., Pedreros, D., Worstell, B., and Verdin, J.: Development of a global slope dataset for estimation of landslide occurrence resulting from earthquakes, Colorado: US Geological Survey, Open-File Report 2007–1188, 2007.

Wang, P., Li, Z., and Gao, W.: Rapid shrinking of glaciers in the Middle Qilian Mountain region of Northwest China during the last ∼ 50 years, J. Earth Sci., 22, 539–548, 2011.

Wei, J., Liu, S., Gou, W., Yao, X., Xu, J., Bao, W., and Jiang, Z.: Surface-area changes of glaciers in the Tibetan Plateau interior area since the 1970s using recent Landsat images and historical maps, Ann. Glaciol., 55, 213–222, 2014.

Yao, T., Thompson, L., Yang, W., Yu, W., Gao, Y., Gou, X., Yang, X., Duan, K., Zhao, H., Xu, B., Pu, J., Lu, A., Xiang, Y., Kattel, D. B., and Joswiak, D.: Different glacier status with atmospheric circulations in Tibetan Plateau and surroundings, Nature Climate Change, 2, 663–667, 2012.

Ye, Q., Zhong, Z., Kang, S., Stein, A., Wei, Q., and Liu, J.: Monitoring glacier and supra-glacier lakes from space in Mt. Qomolangma Region of the Himalayas on the Tibetan plateau in China, J. Mt. Sci., 6, 211–220, 2009.

Zandbergen, P.: Applications of shuttle radar topography mission elevation data, Geography Compass, 2, 1404–1431, 2008.

Zhang, G. Q., Xie, H. J., Kang, S. C., Yi, D. H., and Ackley, S. F.: Monitoring lake level changes on the Tibetan Plateau using ICESat altimetry data (2003–2009), Remote Sens. Environ., 115, 1733–1742, 2011.

Zhang, Y., Liu, S., Xu, J., and Shangguan, D.: Glacier change and glacier runoff variation in the Tuotuo River basin, the source region of Yangtze River in western China, Environ. Geol., 56, 59–68, 2008.

Zwally, H., Schutz, R., Bentley, C., Bufton, J., Herring, T., Minster, J., Spinhirne, J., and Thomas, R.: GLAS/ICESat L2 Global Land Surface Altimetry Data. Version 33. [27° N 72° E, 40° N 105° E], National Snow and Ice Data Center, Boulder, Colorado, USA, 2011.

Title Page

Abstract · Introduction

Conclusions · References

Tables · Figures

◄ · ►│

◄ · ►

Back · Close

Full Screen / Esc

Printer-friendly Version

Interactive Discussion

Table 1. The attributes related to each ICESat measurement.

Name	Attribute description
Time	ICESat-sampling time in "ddMMyyyy" format, derived from the GLA14 attribute i_UTCtime
Lat	Geodetic latitude in degrees, derived from the GLA14 attribute i_lat
Lon	Geodetic longitude in degrees, derived from the GLA14 attribute i_lon
Elev	Elevation in meters above WGS84, derived from the GLA14 attribute i_elev
GdHt	Geoid height in meters in the EGM2008 datum, derived from the GLA14 attribute i_gdHt
SatFlg	Saturation correction flag, identifying possible saturation issues, derived from the GLA14 attribute i_satCorrFlg
NumPk	Number of peaks in the Gauss waveform decomposition from the return echo, derived from the GLA14 attribute i_numPk
SRTM_elev	Elevation in meters above EGM1996, derived from the SRTM DEM data
S	Surface slope in degrees, estimated from the SRTM DEM data
R	Surface roughness in meters, estimated from the SRTM DEM data
96_08_Ht	Geoid height difference between EGM1996 and EGM2008 in meters (Pavlis et al., 2008)
GID	Identification code of the observed glacial area

Table 2. Scenarios of terrain surface parameters for filtering ICESat footprints. Here S_0 and R_0 are terrain slope and roughness thresholds respectively. For each scenario, N is the number of glacial areas observable with a given setting. The numbers $\overline{v}$ and $\overline{\sigma_{vv}}$ are the resulting overall velocity and its propagated standard deviation of glacial elevation change while $\overline{\text{RMSE}}$ is the average of the root mean square errors (RMSEs) of the linear regression model. N_5 is the number of observed glacial areas having a RMSE of below 5 m.

Scenario	S_0 (°)	R_0 (m)	N	$\overline{v}$ (m a^{-1})	$\overline{\sigma_{vv}}$ (m a^{-1})	$\overline{\text{RMSE}}$ (m)	N_5
S1	10	5	33	−0.21	0.20	2.93	29
S2	15	5	38	−0.23	0.21	3.26	34
S3	20	5	43	−0.12	0.21	3.06	40
S4	25	5	49	0.01	0.23	3.34	43
S5	30	5	54	0.04	0.23	4.00	41
S6	10	10	37	−0.25	0.25	2.85	33
S7	15	10	55	−0.06	0.33	2.99	49
S8	20	10	76	−0.02	0.39	3.70	62
S9	25	10	98	0.13	0.44	4.29	68
S10	30	10	117	−0.04	0.45	5.40	67
S11	10	15	39	−0.21	0.26	2.89	36
S12	15	15	63	−0.15	0.40	3.05	58
S13	20	15	90	−0.17	0.47	4.02	67
S14	25	15	122	−0.21	0.56	4.89	64
S15	30	15	146	−0.21	0.61	5.92	57

Table 3. Average glacial change per basin, where N is the number of observed glacial areas and the total glacier area is obtained from the GLIMS glacier mask (Li, 2003). Lost or gained water volumes from glaciers are approximately estimated, by multiplying the average glacial vertical change rate with the total glacier area of each basin.

Basin	Total glacier area (km^2)	N	$\overline{v_B} \pm \overline{\sigma_B}$ (m a^{-1})	Water volume (Gt a^{-1})
Brahmaputra	16 019	9	-0.56 ± 0.49	-8.97 ± 7.79
Ganges	4033	8	-0.99 ± 0.47	-4.01 ± 1.90
Indus	2409	5	-0.03 ± 0.34	-0.08 ± 0.82
Inner plateau	8702	23	-0.16 ± 0.48	-1.39 ± 4.14
Salween	1851	1	-0.78 ± 0.81	-1.44 ± 1.51
Tarim	20 996	39	0.21 ± 0.47	4.31 ± 9.79
Yangtze	2012	5	-1.14 ± 0.46	-2.30 ± 0.93
Total	56 561	90	-0.17 ± 0.47	-9.62 ± 26.41

Table 4. List of pairs of glacial areas that are adjacent, but located on opposite sides of the main mountain ridge. Here N_f is the total number of accepted footprints. Locations A, B, C, D, E and F are indicated in Fig. 8.

No.	Lat.	Lon.	Basin	Ori.	N_f	ICESat tracks	$v \pm \sigma_{vv}$ (ma^{-1})	RMSE
1	28.184	90.544	Brahmaputra	S	261	22	-0.09 ± 0.39	8.68
2	28.248	90.543	Brahmaputra	N	71	9	-0.14 ± 0.40	7.13
3	28.261	86.296	Ganges	S	323	22	-1.83 ± 0.37	3.40
4	28.336	86.302	Ganges	N	93	10	0.12 ± 0.25	4.64
5	30.415	81.306	Ganges	S	80	8	-0.90 ± 0.69	5.83
6	30.469	81.310	Ganges	N	99	8	-0.74 ± 0.54	3.40
7	30.936	83.494	Inner plateau	E	83	9	1.63 ± 0.58	9.21
8	31.022	83.468	Inner plateau	W	160	12	-0.46 ± 0.36	3.56
9	33.913	90.659	Inner plateau	S	92	11	-0.47 ± 0.20	3.92
10	33.954	90.670	Yangtze	N	342	15	-0.60 ± 0.30	3.23
11	34.024	79.763	Indus	SW	79	7	-1.38 ± 0.43	2.73
12	34.053	79.788	Indus	E	185	13	-0.07 ± 0.20	1.51
13	34.288	81.946	Inner plateau	S	106	10	1.23 ± 0.50	2.76
14	34.327	81.946	Inner plateau	N	168	13	0.21 ± 0.47	2.25
15	35.284	80.685	Inner plateau (B)	S	998	34	-1.02 ± 0.29	4.19
16	35.523	80.713	Tarim (A)	N	1320	34	0.69 ± 0.30	3.38
17	35.301	81.430	Inner plateau (D)	SW	635	14	-0.29 ± 0.20	1.73
18	35.388	81.397	Tarim (C)	NE	633	15	-0.09 ± 0.30	1.44
19	35.410	81.612	Tarim (F)	SE	338	14	-0.44 ± 0.44	3.46
20	35.508	81.624	Tarim (E)	N	380	14	0.58 ± 0.28	1.79
21	35.470	82.143	Inner plateau	S	92	9	-1.50 ± 0.79	4.41
22	35.516	82.162	Tarim	N	77	9	-1.02 ± 0.43	5.07
23	35.655	85.620	Inner plateau	S	118	13	1.82 ± 0.48	5.08
24	35.696	85.613	Inner plateau	N	257	13	-0.04 ± 0.24	2.85
25	35.774	77.130	Tarim	W	93	8	0.06 ± 0.57	4.74
26	35.812	77.148	Tarim	N	47	6	0.19 ± 0.57	3.16
27	36.024	90.962	Tarim	S	428	15	-0.80 ± 0.38	7.03
28	36.099	90.936	Inner plateau	N	494	25	-0.55 ± 0.22	2.88
29	36.773	84.903	Inner plateau	S	59	6	-0.13 ± 0.56	2.89
30	36.813	84.895	Tarim	N	52	6	0.03 ± 0.78	2.44

Title Page

Abstract | Introduction

Conclusions | References

Tables | Figures

|◄ | ►|

◄ | ►

Back | Close

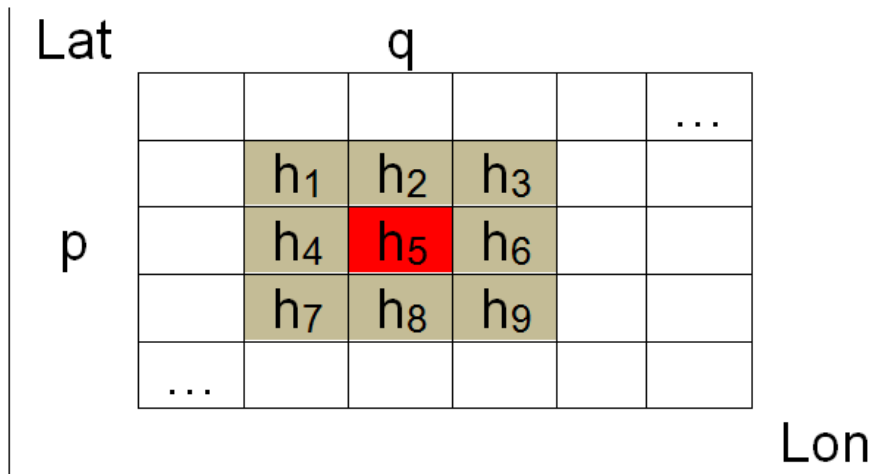Full Screen / Esc

Printer-friendly Version

Interactive Discussion

Table 5. Average glacial vertical change rates per sub-region, where N is the number of observed glacial areas within each sub-region.

Sub-region	Name	N	$\overline{v_R} \pm \overline{\sigma_R}$ (m a^{-1}) this research	ΔH trend on-glacier area (m a^{-1}) Neckel et al. (2014)
A	Western Kunlun Mountains	20	0.16 ± 0.44	0.04 ± 0.29
B	Zangser Kangri and Songzhi Peak	3	0.86 ± 0.31	0.44 ± 0.26
C	Qilian Mountains and Eastern Kunlun Mountains	5	0.03 ± 0.47	-0.90 ± 0.28
D	Tanggula Mountains and Dongkemadi Ice Cap	6	-0.88 ± 0.41	-0.68 ± 0.29
E	Western Nyainqentanglha range	0	NA	-0.23 ± 0.33
F	Gangdise Mountains	8	-0.60 ± 0.50	-0.44 ± 0.26
G	Central and Eastern Tibetan Himalaya	8	-0.70 ± 0.46	-0.78 ± 0.27
H	Eastern Nyainqentanglha and Hengduan Mountains	6	-0.67 ± 0.58	-0.81 ± 0.32
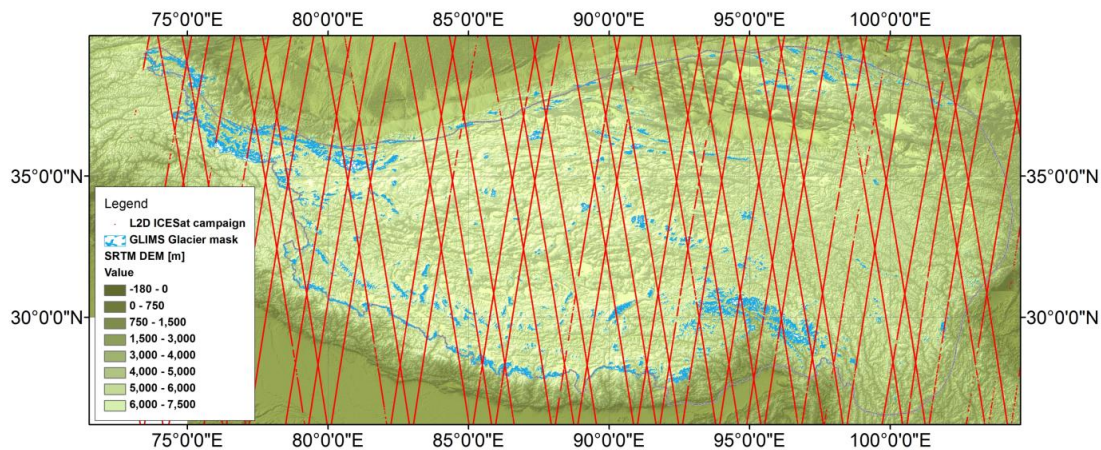
Fig. 1. SRTM elevations, GLIMS glacier outlines and ICESat L2D-campaign tracks.

Fig. 2. Illustration of the 3 by 3 kernel at pixel (p, q), where the h_i values ($i = 1/9$) are corresponding to the DEM elevations.
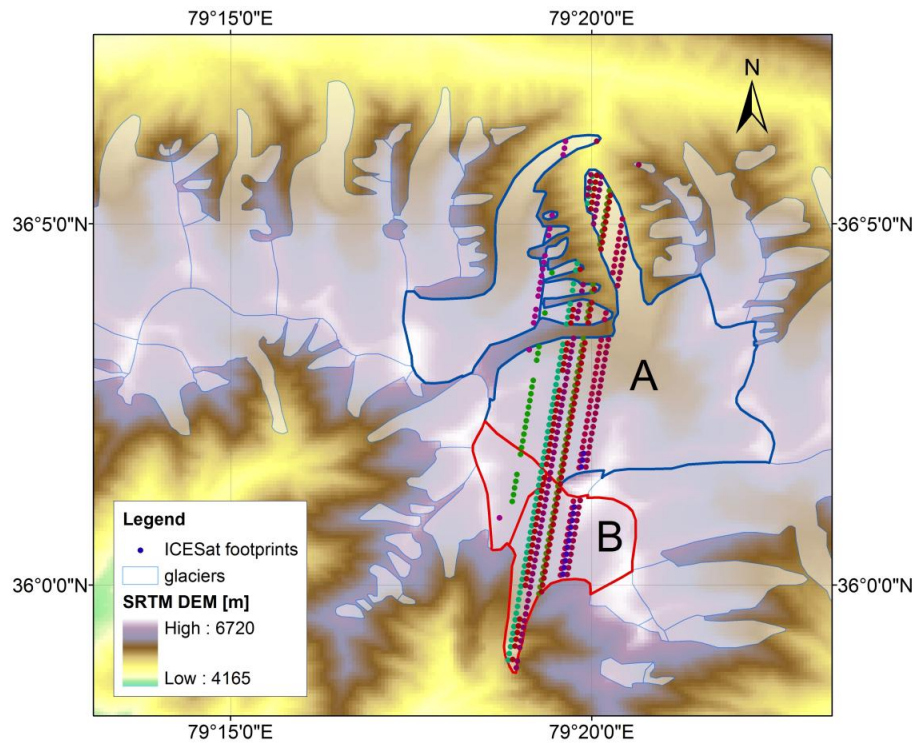
Fig. 3. ICESat footprints superimposed over the GLIMS glacier mask.

$R_A = -1.66 \pm 0.42 \text{ m a}^{-1}$

$R_B = 0.50 \pm 0.31 \text{ m a}^{-1}$

Fig. 4. Glacial vertical changes at the glacial areas A and B between 2003 and 2009.
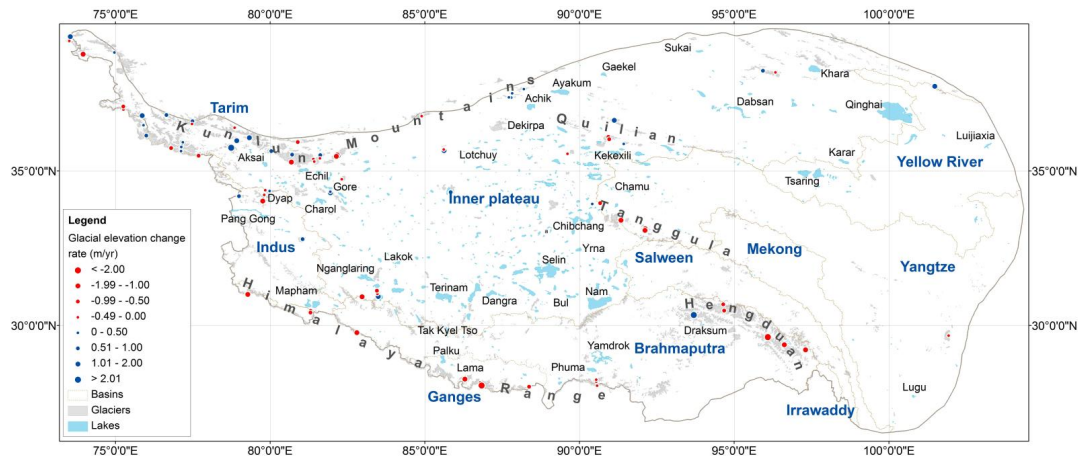
Fig. 5. Glacial vertical changes on the Tibetan Plateau between 2003 and 2009.
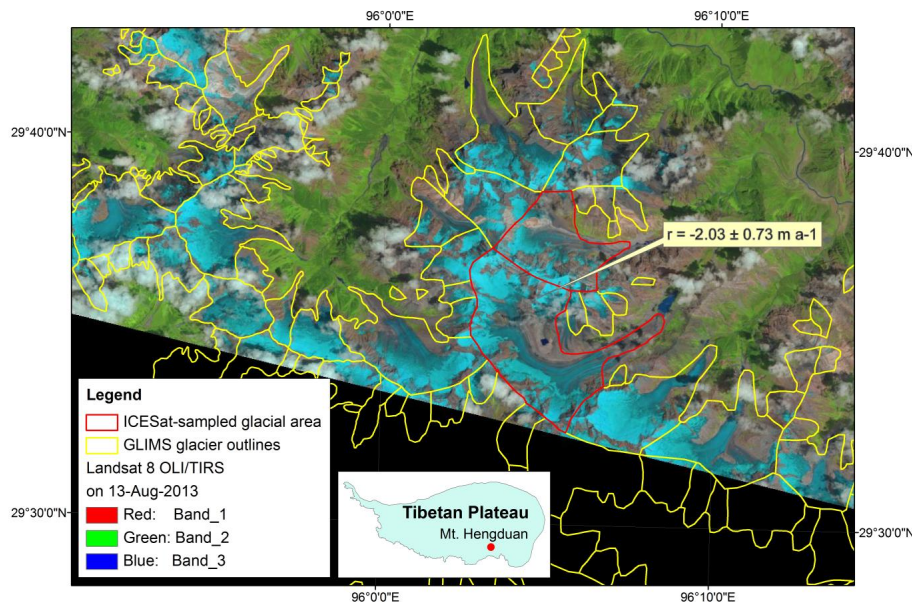
Fig. 6. The maximal rate of glacial vertical decrease between 2003 and 2009 at the Mt. Hengduan. The figure is created by overlaying the GLIMS glacier outlines on the Landsat 8 OLI/TIRS image from 13 August 2013.
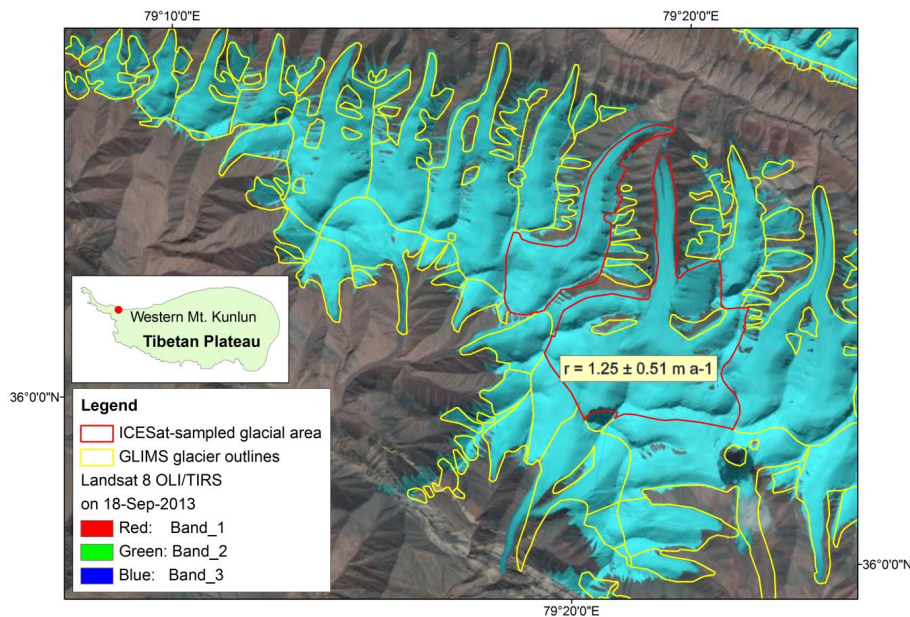
Fig. 7. Strong glacial thickening between 2003 and 2009 at Western Mt. Kunlun. The figure is created by overlaying the GLIMS glacier outlines on the Landsat 8 OLI/TIRS image from 18 September 2013.
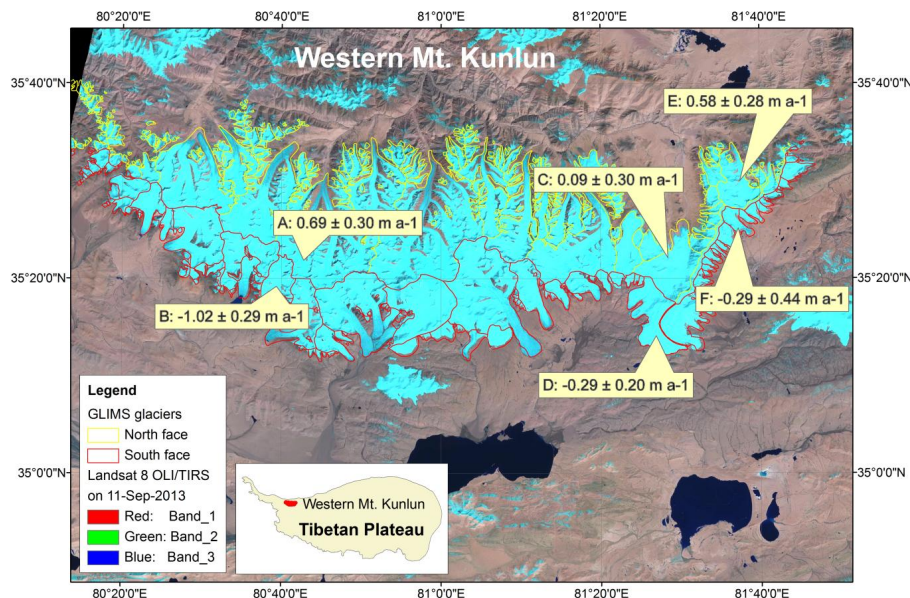
Fig. 8. Different rates of glacial vertical changes between 2003 and 2009 at the North and South face of the Western Mt. Kunlun. The figure is created by overlaying the GLIMS glacier outlines on the Landsat 8 OLI/TIRS image from 11 September 2013, and adding the locations of observed glacial areas with vertical change rates.
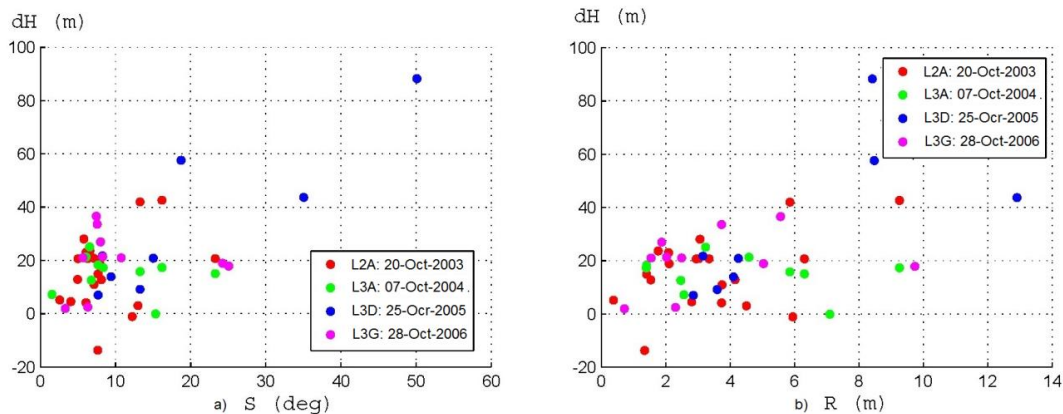
Fig. 9. Relations between **(a)** elevation difference and slope and **(b)** elevation difference and roughness. Elevation differences are between ICESat campaigns L2A, L3A, L3D and L3G and SRTM over a glacial area (Table S1, No. 20 in the Supplement) at the Mt. Guala Mandhata I, belonging to the Ganges Basin.
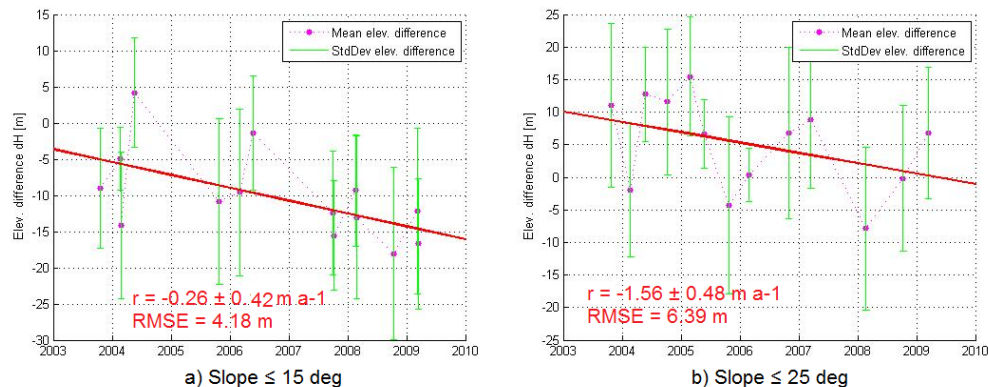
Fig. 10. Estimations of glacial vertial change with varying slope S_0 thresholds: **(a)** 15°, **(b)** 25° at a glacial area (Table S1, No. 6 in the Supplement) in the Hengduan Mountains, belonging to the Brahmaputra Basin. In this example the roughness R_0 was kept fixed at 15 m.

Title Page

Abstract | Introduction

Conclusions | References

Tables | Figures

◄ | ►

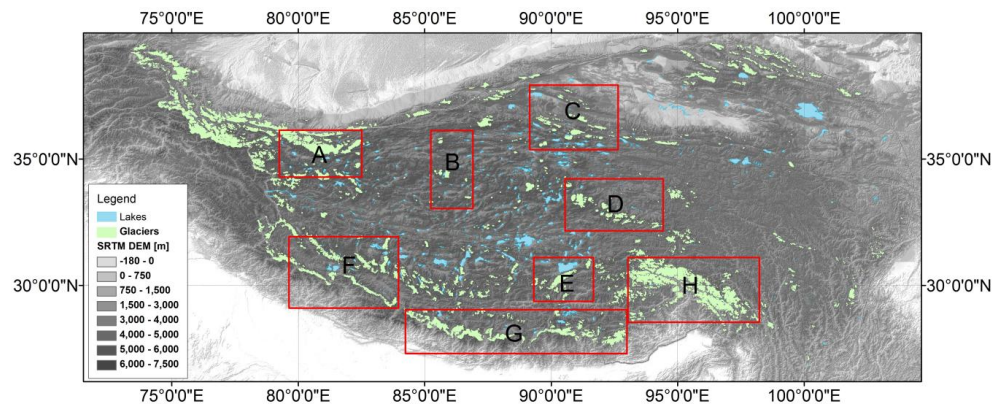◄ | ►

Back | Close

Full Screen / Esc

Printer-friendly Version

Interactive Discussion

Fig. 11. Sub-regions applied for monitoring glacial vertical change, in Neckel et al. (2014).